Liquid Crystals
Publication details, including instructions for authors and subscription information:
http://www.informaworld.com/smpp/title~content=t713926090

Domain manipulation of ferroelectric $BaTiO_3$ thin films: application to the local reorientation of liquid crystal

J. F. Blach[a]; R. Desfeux[a]; A. Da Costa[a]; D. Bormann[a]; J. F. Henninot[a]; M. Warenghem Corresponding author[a]; W. Prellier[b]
[a] Laboratoire de Physico-Chimie des Interfaces et Applications, CNRS FRE 2485, CERLA CNRS FR 2416, Université d'Artois, Rue Jean Souvraz, SP 18, 62307 Lens Cedex, France [b] Laboratoire CRISMAT, CNRS UMR 6508, 6 Boulevard du Maréchal Juin, 14050 Caen Cedex, France

Online publication date: 21 May 2010

To cite this Article Blach, J. F. , Desfeux, R. , Da Costa, A. , Bormann, D. , Henninot, J. F. , Warenghem Corresponding author, M. and Prellier, W.(2004) 'Domain manipulation of ferroelectric $BaTiO_3$ thin films: application to the local reorientation of liquid crystal', Liquid Crystals, 31: 9, 1241 — 1250
To link to this Article: DOI: 10.1080/02678290410001729769
URL: http://dx.doi.org/10.1080/02678290410001729769

LIQUID CRYSTALS, VOL. 31, NO. 9, SEPTEMBER 2004, 1241–1250

Domain manipulation of ferroelectric $BaTiO_3$ thin films: application to the local reorientation of liquid crystal

J. F. BLACH, R. DESFEUX, A. DA COSTA, D. BORMANN, J. F. HENNINOT, M. WARENGHEM*

Laboratoire de Physico-Chimie des Interfaces et Applications, CNRS FRE 2485, CERLA CNRS FR 2416, Université d'Artois, Rue Jean Souvraz, SP 18, 62307 Lens Cedex, France

and W. PRELLIER

Laboratoire CRISMAT, CNRS UMR 6508, 6 Boulevard du Maréchal Juin, 14050 Caen Cedex, France

(*Received 25 June 2003; in final form 10 March 2004; accepted 25 April 2004*)

A method is reported for local alignment of nematic liquid crystal (NLC) molecules. It consists in the poling of small areas of ferroelectric thin films using scanning probe microscopy. A liquid crystal deposited onto such a surface is aligned via a dipole–dipole interaction. The ferroelectric films are first characterized using X ray diffraction, atomic force microscopy and ellipsometry. The domain manipulation and local poling of the film are achieved and characterized using an electrostatic microscopy type set-up. A hybrid nematic liquid crystal cell (NLC-OFC: nematic liquid crystal – oxide ferroelectric cell) is then constructed and its alignment inspected using polarizing microscopy (in reflection mode). The reorientation is explained by invoking a simple interaction between the dipole moment of the LC and the surface electric field generated by the poled area. In addition, a complimentary experiment is performed to determine the depth to which the poled area affects the liquid crystal alignment. This consists of measuring the deflection of a collimated beam (optical soliton) propagating across the poled area.

1. Introduction

The alignment of a liquid crystal by ferroelectric substrates was demonstrated using crystals of a ferroelectric material several years ago. An inspection of the sample via polarized light reveals the domains whatever their origin, either natural [1–5] or induced by stress [6]. A drawback of such an alignment method is the impossibility of controlling the shape of the ferroelectrics domains in such materials. Recently, the alignment of a liquid crystal induced by a large and macroscopically poled area (over $100\,\mu m^2$) of polycrystalline PZT thin films has been demonstrated [7–9]. The manipulation at a sub-micrometer scale of domains of ferroelectric thin films has been demonstrated [10–14] using scanning probe microscopy. From an application point of view in opto-electronics, it is well known that a better integration of a device can be achieved via a thin film approach rather than via bulky materials. In this context, we report experimental results on the alignment of a liquid crystal induced by a poled area in an oriented $BaTiO_3$ thin film. These areas are ferroelectric domains of micron size, created using the scanning probe microscopy (SPM) technique. Such a local alignment of a nematic liquid crystal (NLC) may open new horizons for displays or photonics applications.

One of the attractive features of the $BaTiO_3$ material is its anisotropy, with an associated ferroelectricity at room temperature in the tetragonal phase [15]. In order to use this anisotropy, specific conditions for the control of crystal orientation during growth have been achieved. The preparation of thin films and their characterization using X ray diffraction (XRD), atomic force microscopy (AFM) and ellipsometry are reported in §2 of this paper. Section 3 is devoted to the description of local poling of the $BaTiO_3$ thin film using SPM in contact mode and the NLC cell preparation. The experimental results on NLC alignment by the poled area are reported in §4, together with a simple explanation of the alignment process. Finally a supplementary experiment is reported in §5, which unambiguously shows this NLC alignment.

*Author for correspondence;
e-mail: warenghem@univ-artois.fr

Liquid Crystals ISSN 0267-8292 print/ISSN 1366-5855 online © 2004 Taylor & Francis Ltd
http://www.tandf.co.uk/journals
DOI: 10.1080/02678290410001729769

2. Thin films preparation and characterization

The work presented herein is restricted to $BaTiO_3$ thin films deposited using the laser ablation technique on Pt-$SrTiO_3$ and Pt-MgO substrates.

2.1. *Thin films deposition*

Both the platinum layer and the $BaTiO_3$ thin films were grown by pulsed laser deposition using a KrF excimer laser ($\lambda = 248$ nm). The flux was adjusted to $2\,J\,cm^{-2}$ and the deposition rate close to 3 Hz. During the deposition, the pressure of oxygen was 0.2 Torr and the temperature of the substrate fixed at 720°C. At the end of deposition, the oxygen pressure was increased to atmospheric pressure and then the films were slowly cooled to room temperature. The substrates used for the deposition were (1 0 0)-$SrTiO_3$ (cubic with $a = 3.905$ Å) and (1 0 0)-MgO (cubic, with $a = 4.21$ Å). The number of laser pulses for the Pt layer was 1000 and for the $BaTiO_3$ layer it was 6000 (for the film deposited onto MgO substrate) and 800 (for the film deposited on the $SrTiO_3$ substrate) for the samples studied here.

2.2. *Thin film characterization*

The crystalline structure of the films was characterized using XRD, and the surface morphology using AFM and ellipsometry.

2.2.1. *Crystalline structure of the films by XRD*

Structural characterization by XRD was performed in the (θ–2θ) scan mode using a Rigaku Miniflex+ diffractometer (Cu $K_{\alpha 1}$, $\lambda = 1.5406$ Å). As observed in figure 1, for the film grown on the Pt-$SrTiO_3$, the (θ–2θ) diffraction patterns indicate that the $BaTiO_3$ films grow as a single phase, with the (1 0 0) and (1 0 1) planes parallel to the plane of the substrate. As it is known that the polarization direction of $BaTiO_3$ is parallel to the *c*-axis, we conclude that the domain structure of the film comprises domains with an in-plane polarization, (1 0 0) domains, and domains with an out-of-plane polarization, (1 0 1) domains. No peak characteristic of other phases appears. As deduced from the XRD patterns, the *a* and *c* lattice parameters of the tetragonal $BaTiO_3$ cell have been calculated to be 3.99 and 4.02 Å, respectively. These values are in agreement with structural distortions of the tetragonal cell when compared with literature data [16]. These results are valid for both samples studied here.

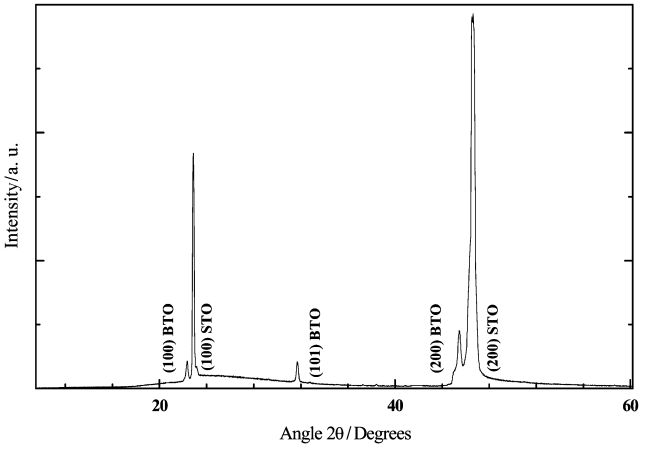

Figure 1. X-ray diffraction patterns of $BaTiO_3$ (BTO) thin film (800 pulses) deposited on a platinized $SrTiO_3$ (STO) substrate.

2.2.2. *Morphological study by AFM and ellipsometry*

AFM measurements were carried out in air at room temperature using a Park Autoprobe CP scanning force microscope which operates with an optical deflection sensor force. The AFM images for surface morphology and grain size analysis were obtained in the contact mode with Si ultralever tips. Figure 2 shows typical 2D and 3D images of the surface of the $BaTiO_3$-Pt-$SrTiO_3$ film. We observe for the two films a classic island growth surface morphology, typical of a Volmer–Weber or Stranski–Krastanov growth mode [17]. The surface is dense and exhibits grains with good connectivity, with a size of around 530 Å on Pt-$SrTiO_3$ and 540 Å on Pt-MgO. The root mean square roughness of the film, measured on different $1 \times 1\,\mu m^2$ scanned areas, was around 22 and 67 Å for the $BaTiO_3$-Pt-$SrTiO_3$ and $BaTiO_3$-Pt-MgO films, respectively. The average peak to valley surface roughness are about 204 and 470 Å for the $BaTiO_3$-Pt-$SrTiO_3$ and $BaTiO_3$-Pt-MgO films respectively.

Spectroscopic ellipsometry (SE) measurements were performed using a Jobin–Yvon UVISEL HR 460 ellipsometer. Spectra were recorded in the visible range (400–800 nm). To extract thickness and roughness from these data, they were compared and fitted to a three layered sample model, as shown in figure 3, including a rough overlayer as reported by Jellison *et al.* [18]. The optical function of the substrate entered in the overall model was experimentally obtained from spectra recorded on bare substrates prior to thin layer deposition, and fitted using a Sellmeier transparent dispersion formula. The optical function of platinum was found in the literature [19]. The $BaTiO_3$ was considered as an isotropic film since the size of the mono-domains is small [20] compared with the illuminated area, and randomly distributed across this area. We performed the fit using the $BaTiO_3$ optical function found either in the literature [18, 21, 22] or the fit itself which yields to it, both approaches yielding the

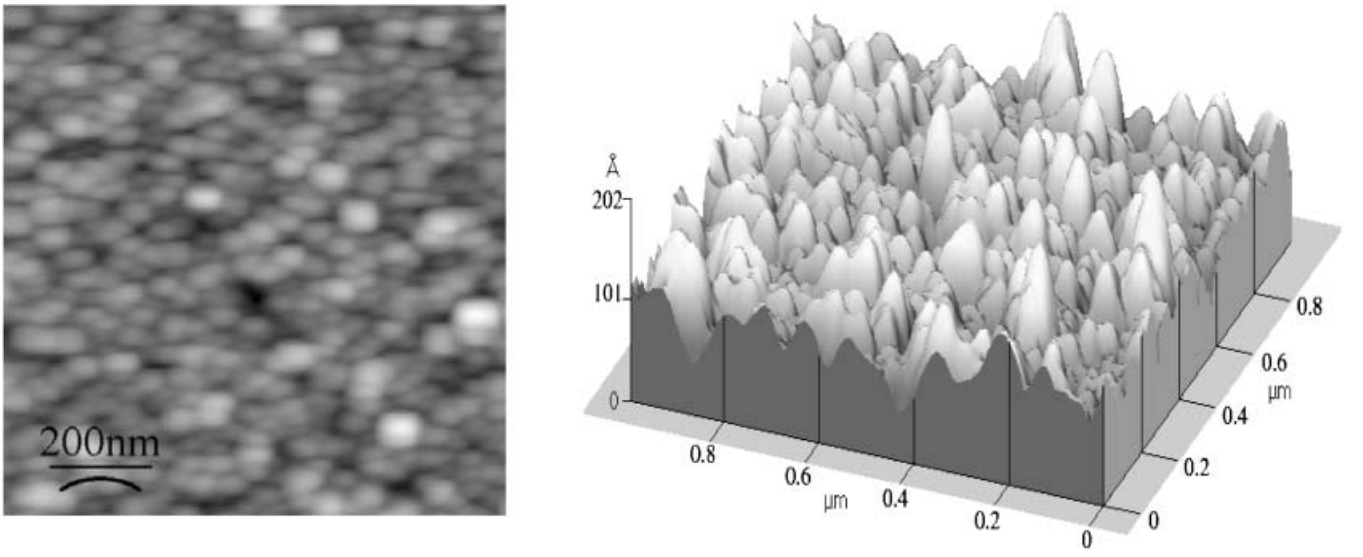

Figure 2. 2D (left) and corresponding 3D (right) AFM images of typical areas of $BaTiO_3$ films grown on $SrTiO_3$ substrates showing an island-like surface morphology. The scan area is $1 \times 1\,\mu m^2$.

same results for the thickness of the film and its roughness. For the 800 pulses $BaTiO_3$ film, the best fit results for the thicknesses of the rough layer and the film itself are 200 and 770 Å respectively, whereas for the 6 000 pulses film they are 190 and 6 590 Å. Thus SE gives a good estimation of the thickness of the BTO film, correlated to the pulse number.

3. Poling and hybrid nematic liquid crystal – oxide ferroelectric cell (NLC–OFC)

The films were submitted to local domain manipulation (local poling or writing). The poled area was checked (reading) using the electrostatic force microscopy (EFM) mode; it was then covered with a liquid crystal, and a LC cell constructed as described next.

3.1. *Domain manipulation*

For this preliminary experiment, simple patterns (squares) were tested. The poling (writing by SPM) and the reading by EFM were carried out in air, at room temperature, using a Park Autoprobe CP. The EFM technique measures the residual surface charge density of the ferroelectric film by probing the electrostatic interaction between the metallic tip and the charge distribution on the ferroelectric surface [13, 23, 24]. In the first step (writing), a voltage is applied ($U_{pol} = \pm 10.5$ V) between the tip and the sample which is displaced, scanning different squared areas ($7.5 \times 7.5\,\mu m^2$) in contact mode. The second step (reading) consists of recording the EFM image on a larger scale. To visualize the ferroelectric domains, an a.c. modulation signal was applied between the conductive tip and the Pt layer, the tip operating in the non-contact mode. Silicon microlever tips overcoated with cobalt were used. The photodetector signal was entered simultaneously into a lock-in amplifier and into the z-control feedback of the AFM system [13]; the lock-in amplifier detects the first harmonic signal. Both signals were recorded, giving simultaneously a topographic image and an EFM image. In our system, an a.c. modulation signal of 1 V at 17 kHz was used for the imaging. To check the reversibility of the poling, we

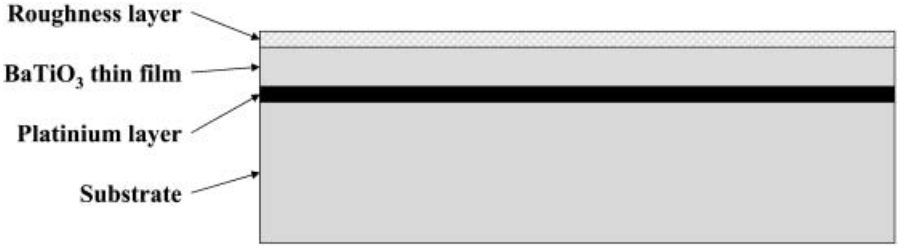

Figure 3. Schematic representation of the structure entered in the model for spectroscopic ellispometry data fitting.

have successively written two squares, partially overlapping each other, the first with a positive applied voltage (+10.5 V) and the second with a negative voltage (−10.5 V). The result is shown in figure 4, read on an enlarged area ($16 \times 16\,\mu m^2$) including the polarized areas [12, 13, 24]. The white square fully overwrites the black one, demonstrating that the poling is a reversible phenomenon. In conclusion, it is possible to obtain a homogeneouly poled area at the micron scale at the surface of the thin film using scanning probe microscopy.

3.2. *The hybrid cell design*

In order to check the influence of the poled areas created in the thin film by SPM on a layer of nematic liquid crystal (NLC), hybrid liquid crystal cells were prepared, as schematically shown in figure 5. Mylar® spacers, 10 and 23 μm, were used to adjust the NLC layer thickness. The planar alignment of NLC on the upper glass was achieved using a conventional unidirectional rubbed polymer coating (PVA). The cell was then sealed with Araldite® epoxy and filled with a commercial liquid crystal (K15 from Merck, pentylcyanobiphenyl 5CB) in the nematic phase. For some samples, the poled area was checked (reading) using EFM before glueing the cell, otherwise the cell was filled immediately after the writing process in order to prevent the poling from damping [23]. The cells were inspected using a polarizing microscope as reported next.

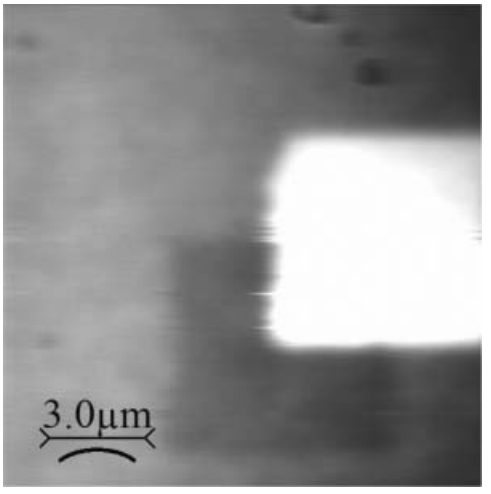

Figure 4. EFM images of the surface of a $BaTiO_3$ film on which has been polarized first a square with a positive voltage (dark zone) and then a second square with a negative voltage (white zone) (±10.5 V).

4. Experimental observation of the NLC-OFC and LC alignment analysis

We first report on the observation of the influence of the poled area on the LC alignment, then describe the possible mechanisms responsible for this alignment, and finally propose a structure of the cell.

4.1. *Observations*

Two cells were prepared, both with a squared poled area ($50 \times 50\,\mu m^2$). One was constructed using the 'thick' $BaTiO_3$ film (6000 pulses) and 23 μm mylar spacers, and a second one using the 'thin' $BaTiO_3$ film (800 pulses) and 10 μm mylar spacers. The cells were observed using an Olympus BH-2 polarizing microscope (reflection mode) a few minutes after their preparation to allow the NLC defects to relax; the results are shown in figures 6(*a*) and 7(*a*), respectively. In both cases, the square pattern is clearly revealed. In figure 6(*a*), a schieleren texture can be seen, characteristic of the nematic phase, surrounding the square area, which is black when the crossed polarizers of the microscope are parallel to the sides of the poled area and white for any other orientation of the sample with respect to the crossed polarizers; i.e., this poled area is a uniaxial block. It is worth noting that the direction of the optical axis (projection) is not that of the rubbing

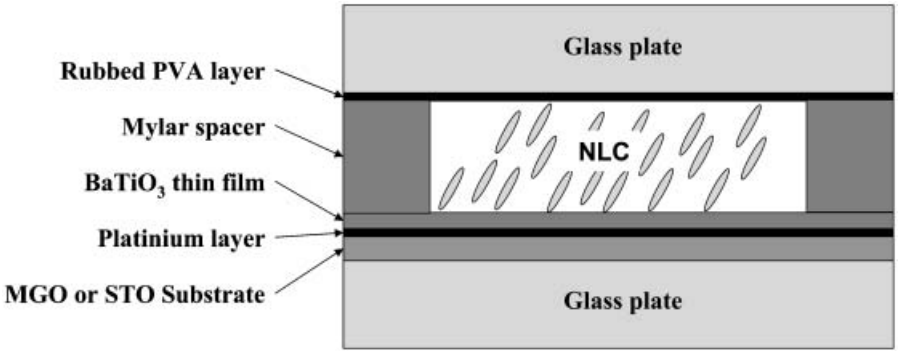

Figure 5. Schematic representation of the hybrid liquid crystal – $BaTiO_3$ cell.

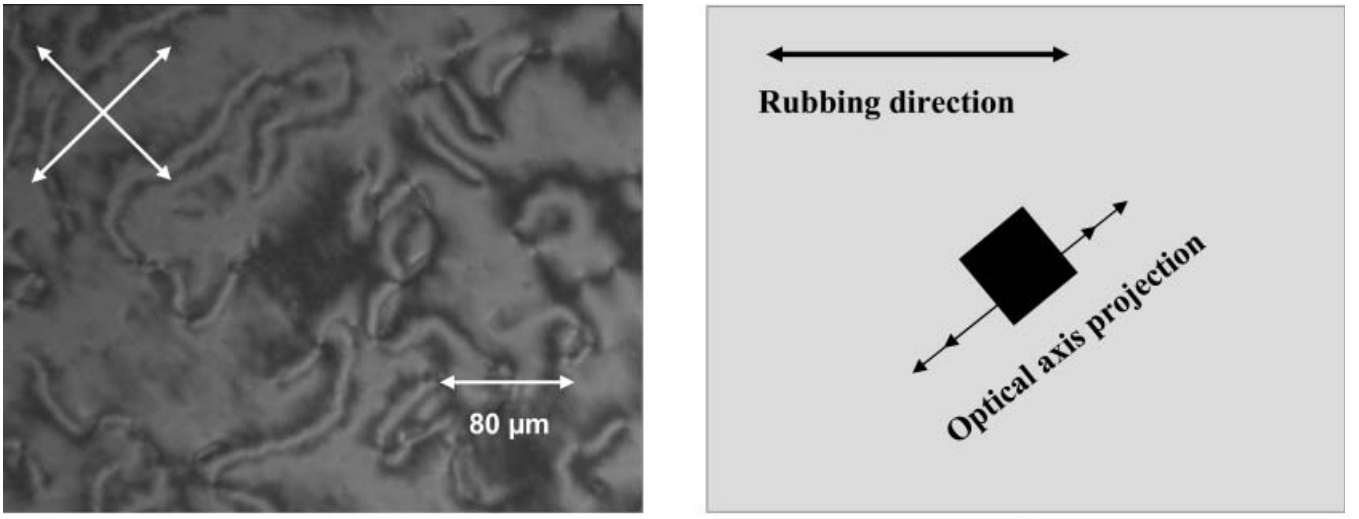

Figure 6. 'Thick' $BaTiO_3$ cell (6 000 pulses; 659 nm): (*a*) polarizing microscopy images; (*b*) sketch of the main direction, as deduced from experimental analysis using polarizing microscopy.

axis but that of the AFM scanning used during the writing process, as shown schematically in figure 6 (*b*). This example shows that the poled area clearly influences the alignment of the LC.

In figure 7 (*a*), although the poled area is clearly visible at a glance, closer examination shows that the texture is the same outside and inside the poled area: a black background, studded with grey splashes. These splashes are brighter within the poled area than outside it. Upon rotation of the sample, the background becomes brighter as the rubbing direction moves away from that of the crossed polarizers, simultaneously inside and outside the poled area. However, the splashes change from bright to dark inside the poled area, whereas they change from bright to grey outside it. In addition, the maxima (minima) of reflected light from these splashes occur for positions of the sample with respect to the crossed polarizers which are different inside and outside of the poled area, revealing a corresponding difference in alignment of the LC around these spots. The general situation of optical axis is shown in figure 7 (*b*). In conclusion, for both cells, the poled area induces a local alignment of the LC.

4.2. *Discussion*

There are two questions still to answer: first, the simple visual inspection through the microscope does

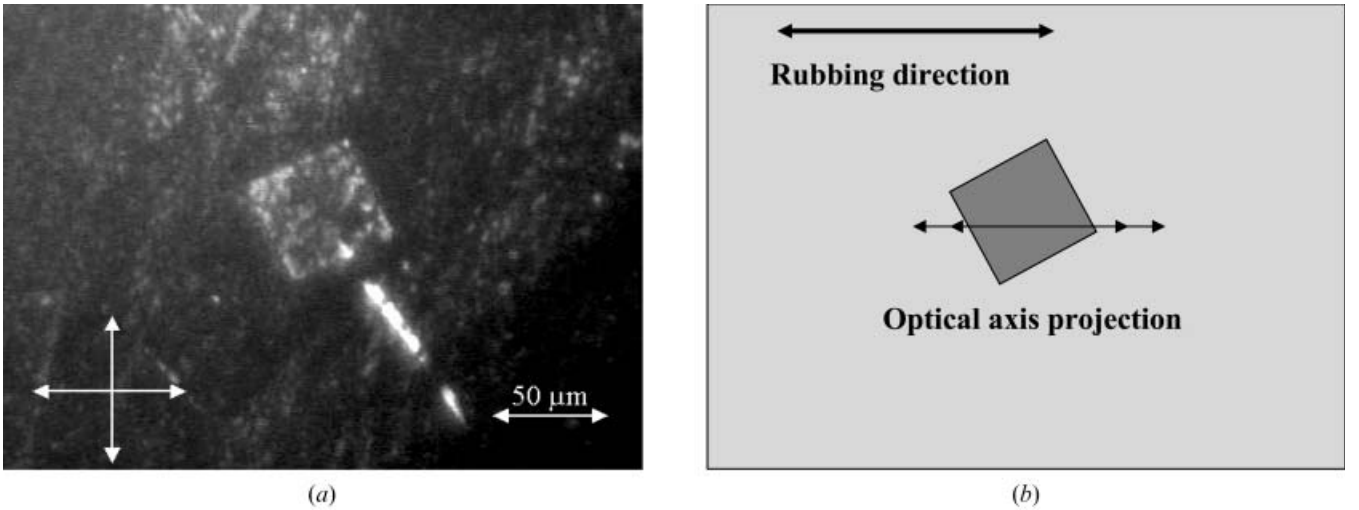

Figure 7. 'Thin' $BaTiO_3$ cell (800 pulses, 77 nm): (*a*) polarizing microscopy images; (*b*) sketch of the main direction, as deduced from experimental analysis using polarizing microscopy.

not allow us to discriminate between a fully planar zone and a hybrid one; second, the fact that the optical axis projection is parallel to the rubbing direction in the second case, and parallel to the scanning direction in the first, is intriguing. The first question will be addressed in the next section via an additional experiment. Let us consider the second question. To explain these observations, we first note that the $BaTiO_3$ film consists of sub-micron scale domains as commonly reported for ferroelectric films [14, 25]; some with dipoles pointing outward or inward of the interface, (1 0 1) domains, and some with in-plane dipoles, (1 0 0) domains. As an approximation, both the normal and tangential components of the surface electric field, $\mathbf{E}_s$, generated by the dipoles statistically vanishes. As a result, there is no preferred direction for the director of the LC to align along and the anchoring of the LC is degenerate on these substrates: the overall alignment of the LC is ruled by the other interface, namely a planar one, on condition that the thickness is not too large. This is what we observe outside the poled area: the thick LC sample contains defects, figure 6 (*a*), whereas the thin one is homogeneously planar, figure 7 (*a*).

Let us now consider the poled area and a simple picture of the writing process. During this step, a writing field $\mathbf{E}_w$ is applied between the tip and the Pt layer. It is mostly perpendicular to the surface, figure 8 (*a*). Under the influence of the writing field, the dipoles of the (1 0 1) domains, which are tilted with respect to the interface, switch in order to minimize the dipole/electric field coupling energy and thus point upward or downward with respect to the interface, according to the electric field direction. This organization of the dipoles is quasi-permanent and those dipoles generate a non-zero perpendicular component of the surface electric field $\mathbf{E}_s$ in this area. Its intensity is obviously correlated with the number of dipoles, thus the larger the thickness of the $BaTiO_3$ film, the larger the perpendicular component.

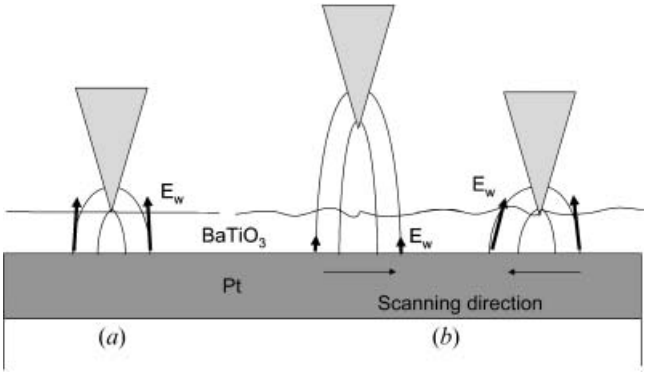

Figure 8. Sketch of the electric field during the writing process: (*a*) perfect situation, flat surfaces and steady tip; (*b*) scanning sample, no flat surface and contact mode for one way.

In such an ideal picture, the tangential component of the $\mathbf{E}_s$ is randomly oriented and thus vanishes; in addition, the in-plane dipoles–(1 0 0) domains—are perpendicular to the writing field and do not interact with it. There are, however, several secondary phenomena that can induce a coupling of these in-plane dipoles with the writing field, yielding a non-zero tangential component of $\mathbf{E}_s$ directed along the scanning direction. First, AFM and ellipsometry measurements show that the surface is not perfectly flat: some in-plane dipoles are no longer perpendicular to the writing field and can couple with the writing electric field. Second, during the writing process, the sample is moving back and forth along the scanning direction, the tip being in contact only in one way; the distribution of the writing field is thus unlikely to be symmetric, with a preferred tangential component of $\mathbf{E}_w$ along the scanning direction. Finally, while in contact with the film, the tip provides the surface with some mechanical energy that helps to break up the metastability of the in-plane dipoles with respect to the writing field. All these effects—shown schematically in figure 8 (*b*)—act the in same way: breaking the symmetry along the scanning direction, and inducing, via in-plane dipole reorientation, an in-plane component of the surface electric field parallel to the scanning direction.

The study of the exact role of each process is beyond the scope of this paper, however the tangential component of the surface electric field is most probably correlated with the roughness of the surface, and given the thick $BaTiO_3$ film is more than twice as rough as the thin one, one expects a larger tangential component for it. In conclusion, we expect a surface electric field in the poled area with a component perpendicular to the surface (correlated with the thickness of the $BaTiO_3$ film) and one tangential to it (correlated with the roughness of the $BaTiO_3$ film), in the scanning direction. Schematically the (1 0 0) domains contribute to the tangential component and the (1 0 1) domains to the perpendicular component.

4.3. *Proposed structures*

We suggest therefore that the LC director is aligned along the surface electric field according to a Freedericksz process [26], the dielectric anisotropy of the material used being positive. The anchoring energy at this interface is larger for a larger surface electric field, and thus larger for a larger thickness of the ferroelectric layer. This explains the observed director distributions of the LC, as shown in figures 6 and 7. For the thick

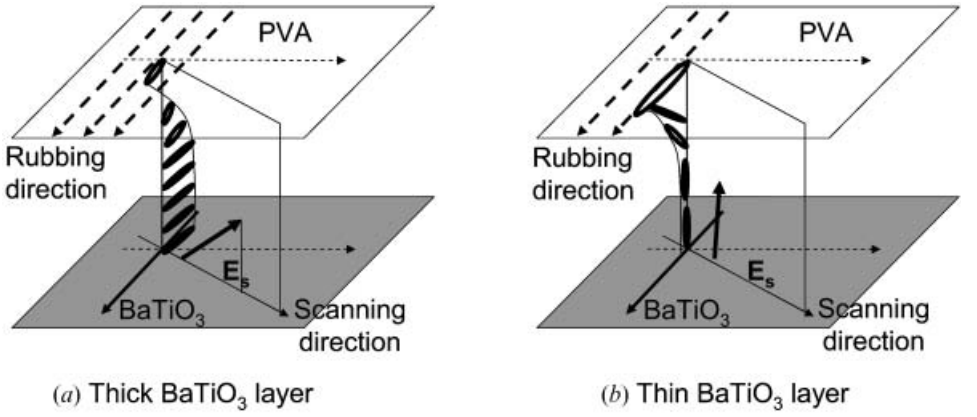

Figure 9. Proposed structures for the cells shown in (*a*) figure 6, and (*b*) figure 7.

ferroelectric film (figure 6), both components—tangential (roughness) and perpendicular (thick)—of the surface field are large and induce a tilted alignment of the LC with a strong equivalent anchoring energy, overcoming the planar alignment induced by the upper plate of the cell, as shown schematically in figure 9 (*a*). This explains the direction of the projection of the optical axis, which is parallel to the scanning direction. By contrast, the thinner ferroelectric film of the cell shown in figure 7 having a smaller roughness, the tangential surface electric field is small, i.e., this field is practically perpendicular to the surface. One thus expects a quasi-homeotropic alignment of the LC on this poled area, with an equivalent anchoring energy smaller than that obtained with a thicker ferroelectric film. In addition, with the thickness of the cell being smaller, the upper polymer coating easily prevents the overall alignment of the LC in the cell, figure 9 (*b*); this explains why the direction of the projection of the optical axis is parallel to the rubbing direction. Nevertheless, simple optical inspection of the sample via polarizing microscopy does not allow us to ascertain whether the alignment is fully planar or hybrid as suggested in figure 9 (*b*); thus, for the cell shown in figure 7, we cannot conclude whether or not the poled area really influences the LC alignment. Although the splashes respond differently inside and outside the poled area upon rotation of the cell around the optical axis of the microscope, leading us to suppose that the poled area affects the NLC alignment, we decided to undertake an extra experiment on that cell to clarify this point.

5. Cross-check experiment: beam deflection

The experiment consists of launching a beam in the NLC material from a lateral side of the cell and checking its behaviour as it crosses the poled area. Any deviation of that propagation will reveal a change in the index of refraction and thus a change of orientation of the NLC director. Moreover, a gaussian distribution of light, such as a laser beam, is more absorbed in its centre than in its external part, thus the central part is hotter than the external part of the beam and experiences a different index of refraction, resulting in its focusing or defocusing depending on the dn/dT sign. Our NLC material is such that an ordinary wave is focused ($dn_o/dT > 0$), whereas the extraordinary beam is defocused ($dn_e/dT > 0$) [27]. Therefore, a gaussian beam crossing an interface splitting two anisotropic media having their optical axes respectively perpendicular and parallel to the linear polarization direction of the beam will experience a change from focusing to defocusing, which is easier to detect than a mere small deflection. We performed the experiment using the set-up schematically depicted in figure 10. The green line (532 nm) of an Nd-V_2O_4 laser is introduced into the NCL cell via a single-mode fibre, placed on translation stages in order to allow the correct positioning of the beam with respect to the poled area. The set-up is placed on a microscope stage and the light scattered by the LC is collected via the microscope, revealing the beam behaviour as it freely propagates in the LC medium. We doped the NLC with a small amount of dye (quininzarin, 0.3 wt %) to enhance the thermal non-linear capability of the material and to launch a collimated beam [28]. Such a collimation can be achieved for an input power in the range of mW and an input beam linearly polarized to excite the ordinary wave in the NLC material. The polarization is controlled via a three-loop system and is properly aligned with respect to the NLC optical axis.

In figure 11, a deflection and a fanning-out is clearly visible, indicating without doubt that the poled area induces a strong realignment of the NLC. A closer look at (figure 11 (*b*)) shows that only part of the beam is

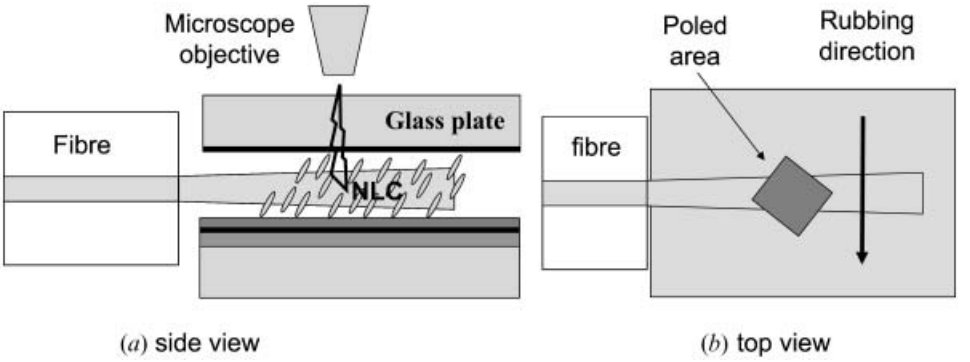

Figure 10. Set-up to probe the NLC alignment induced by the poled area: (*a*) side view, (*b*) top view. The probe beam is linearly polarized perpendicular to the plane of figure 10 (*b*).

deflected. This can be explained by considering the proposed structure in figures 7 (*b*) and 12 in which the cell in the poled area is hybrid. The probe beam has a diameter of around 7 μm and thus crosses practically the whole cell thickness. Outside the poled area, the beam travels through planarly aligned material, with polarization perpendicular to the optical axis (ordinary wave). As it enters the poled area, the lower part of the beam is polarized parallel to the optical axis and thus becomes an extraordinary wave, whereas the upper part remains polarized perpendicular to the optical axis and thus remains an ordinary wave, as shown schematically in figure 12 (*b*). The upper part keeps propagating in a collimated fashion, whereas the lower part is deflected according to Snell's law and is defocused, fanning-out due to its non-linear property. Since quite a large amount of light is clearly deflected, the influence of the poled area on the NLC alignment is not negligible, in other words, the quasi-homeotropic alignment induced by the $BaTiO_3$ film extends over a reasonably large thickness (anchoring energy quite large). The deflection can be roughly estimated by applying Snell's law with the ordinary and extraordinary indices of 5CB ($n_o = 1.53$; $n_e = 1.72$) and a 45° incidence: this gives a 7° deflection. To this deflection, must be added the fanning-out (defocusing) which is around 15° for the input power considered [26]. The envelope of the beam is therefore deflected to around 22° which is very close to the deflection measured (20°–24°) on the photograph shown in figure 11. The agreement is quite good, with the condition that the beam is fully extraordinary (maximum index and maximum dn_e/dT); i.e. the alignment induced by the poled area is homeotropic, not tilted.

6. Conclusion

Oriented $BaTiO_3$ thin films have been grown on Pt-$SrTiO_3$ and Pt-MgO substrates. The structural and morphological properties of the thin films were studied using various techniques (XRD, AFM and ellipsometry). It is found that the thin film structures consist of

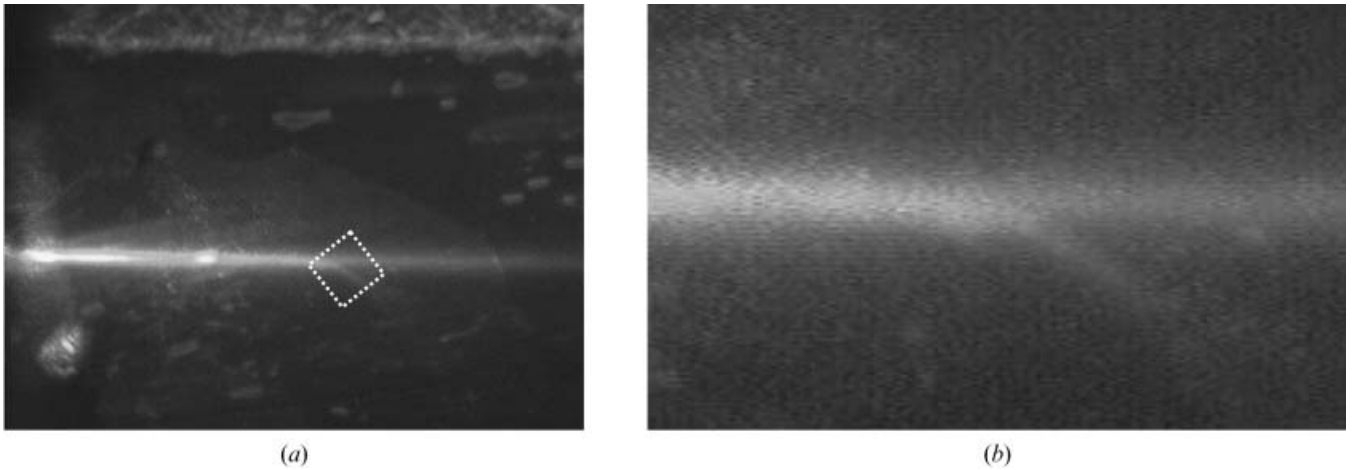

Figure 11. Visualization of the deflection: the focusing/defocusing of a probe beam crossing the poled area. (*a*) General view, the poled area is visualized by the dotted line (side 50 μm); (*b*) close view.

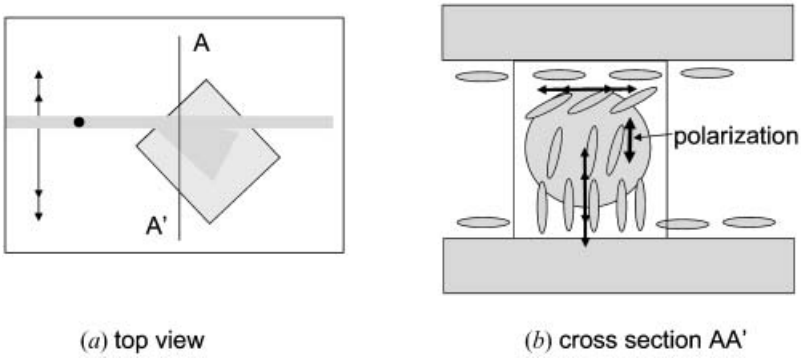

Figure 12. Sketch showing the different direction of axis: (*a*) top view, (*b*) cross-section. The double arrow represents the optical axis; the polarization of the beam is shown by a dot in (*a*) and a single arrow in (*b*). The grey circle represents the cross-section of the beam.

sub-micron sized domains with (1 0 0) and (1 0 1) planes parallel to the substrate plane; that is, with dipoles lying in the surface (1 0 0) domains and dipoles pointing out of the interface (1 0 1) domains. The possibility of poling the films using SPM (polarization experiments and EFM investigations) is demonstrated, and the strong action of these poled area on the LC alignment as shown by well. Using them as a substrate to prepare hybrid aligned liquid crystal cells. It is found that the poled area induces a tilted or homeotropic alignment, via a coupling to the surface electric field (Fréedericksz process). The influence of this reorientation is found to be stronger than that of the polymer coating on the other plate of the cell. The thickness of the ferroelectric film, being closely linked to the surface electric field, plays a major role in the strength of the LC reorientation (equivalent anchoring energy). In addition, a beam travelling though the LC, parallel to the ferroelectric film, is shown to experience some deflection, revealing that the influence of the poled area extends over a reasonably large thickness of the LC, and showing the possibility of manipulating the beam. This opens a new prospect in generating micro/nano patterns in liquid crystal-based devices, of especial interest in photonics.

The LPCIA participates in the Centre d'Etudes et de Recherches Lasers et Applications (CERLA) supported by the Ministère chargé de la Recherche, the Région Nord-Pas de Calais and the Fonds Européen de Développement Economique des Régions.

References

[1] NAKATANI, N., and HIROTA, M., 1981, *Jpn. J. appl. Phys.*, **20,** 2281.
[2] FURUHATA, Y., and TORIYAMA, K., 1973, *Appl. Phys. Lett.*, **23,** 361.
[3] GLOGAROVA, M., JANOVEC, V., and TIKHOMIROVA, N. A., 1979, *J. Physique*, **40,** 502.
[4] KONSTANTINOVA, V. P., TIKHOMIROVA, N. A., and GLOGAROVA, M., 1978, *Ferroelectrics*, **20,** 259.
[5] TIKHOMIROVA, N. A., SHUVALOV, L. A., BARANOV, A. I., KARASEV, A. R., DONTSOVA, L. I., POPOV, E. S., SHILNIKOV, A. V., and BULATOVA, L. G., 1980, *Ferroelectrics*, **29,** 51.
[6] LUPASCU, D. C., DOS SANTOS E LUCATO, S. L., RODEL, J., KREUZER, M., and LYNCH, C. S., 2001, *Appl. Phys. Lett.*, **78,** 2554.
[7] HUBBARD, J. F., GLEESON, H. F., WHATMORE, R. W., SHAW, C. P., ZHANG, QI., and MURRAY, A. J., 1999, *Mol. Cryst. liq. Cryst.*, **329,** 491.
[8] HUBBARD, J. F., GLEESON, H. F., WHATMORE, R. W., SHAW, C. P., and ZHANG, QI., 1999, *J. mater. Chem.*, **9,** 375.
[9] ROY, S. S., GLEESON, H. F., SHAW, C. P., WHATMORE, R. W., HUANG, Z., ZHANG, Q., and DUNN, S., 2000, *Integrated Ferroelectrics*, **29,** 189.
[10] AHN, C. H., TYBELL, T., KUFFER, O., ANTOGNAZZA, L., CHAR, K., HAMMOND, R. H., BEASLEY, M. R., FISHER, O., and TRISCONE, J.-M., 1998, *Mater. Sci. Eng. B*, **56,** 173.
[11] CHEN, X. Q., YAMADA, H., TERAI, Y., HORIUCHI, T., MATSUSHIGE, K., and WEISS, P. S., 1999, *Thin solid Films*, **353,** 259.
[12] LANDAU, S. A., JUNGHANS, N., WEISS, P.-A., KOLBESEN, B. O., OLBRICH, A., SCHINDLER, G., HARTNER, W., HINTERMAIER, F., DEHM, C., and MAZURÉ, C., 2000, *Appl. surface Sci.*, **157,** 387.
[13] SHIN, H., LEE, K., MOON, W. K., JEON, J. U., LIM, G., PAK, Y. E., PARK, J. H., and YOON, K. H., 2000, *IEEE Trans. Ultrason.*, **47,** 801.
[14] PARUCH, P., TYBELL, T., and TRISCONE, J. M., 2001, *Appl. Phys. Lett.*, **79,** 530.
[15] SRIKANT, V., TARSA, E. J., CLARKE, D. R., and SPECK, J. S., 1995, *J. appl. Phys.*, **77,** 1517.
[16] The value is in good agreement with the JCPDS value: *Powder Diffraction Files Phases—Inorganic Phases* (Center for Diffraction Data, PA,1998) Card N° 05-0626 where $a = 3.994$ Å and $c = 4.036$ Å.
[17] VOOK, R. W., 1982, *Int. Metals Rev.*, **27,** 209.
[18] JELLISON, G. E., BOARNER, L. A., LOWNDES, D. H., MCKEE, R. A., and GODBOLE, M., 1994, *Appl. Opt.*, **33,** 6053.
[19] PALIK, E. D., 1998, *Handbook of Optical Constants of Solids* (Academic Press).

[20] BLACH, J. F., BORMANN, D., DESFEUX, R., WARENGHEM, and PRELLIER, W., 2003, *J. Physique IV* (to be published).
[21] WEMPLE, S. H., DIDOMENICO, M., and CAMLIBEL, JR, I., 1968, *J. Phys. Chem. Solids*, **29,** 1797.
[22] DIDOMENICO, M., and WEMPLE, JR., S. H., 1968, *Phys. Rev.*, **166,** 565.
[23] TYBELL, T., AHN, C. H., and TRISCONE, J.-M., 1999, *Appl. Phys. Lett.*, **75,** 856.
[24] JO, W., KIM, D. C., and HONG, J. W., 2000, *Appl. Phys. Lett.*, **76,** 390.
[25] HIKADA, T., MARUYAMA, T., SAITOH, M., MIKOSHIBA, N., SHIMIZU, M., SHIOSAKI, T., WILLS, L. A., HISKES, R., DICAROLIS, S. A., and AMANO, J., 1996, *Appl. Phys. Lett.*, **68,** 2358.
[26] FRÉEDERICKSZ, V., and ZOLINA, V., 1933, *Trans. Faraday Soc.*, **29,** 919.
[27] KHOO, I. C., and SIMONI, F., 1991, *Physics of Liquid Crystlline Materials* (Gordon & Breach).
[28] HENNINOT, J. F., DEBAILLEUL, M., DERRIEN, F., ABBATE, G., and WARENGHEM, M., 2001, *Synth. Met.*, **124,** 9.